Spring 2021

Redox-Active Coordination Complexes for Small Molecule Activation with Environmental Applications

Hanalei Lewine
Western Washington University

Redox-Active Coordination Complexes for Small Molecule Activation with Environmental Applications

Hanalei Lewine, Dr. John D. Gilbertson
Department of Chemistry, Western Washington University,
516 High Street MS 9150, Bellingham, WA 98225
lewineh@wwu.edu

Abstract

Nitrate and nitrate are harmful pollutants resulting from the overuse of nitrogen fertilizers in agriculture. The pyridinediimine ligand scaffold with a hemilabile pendant phosphine shows reactivity towards these species to selectively reduce them to NO on a mononuclear iron complex (MNIC). Experimental work is supported by DFT broken symmetry calculations.

Introduction

The invention of the Haber-Bosch process in the early 20th century allowed atmospheric nitrogen to be converted to ammonia (NH_3), forming the basis of nitrogen fertilizers.[1] While this innovation enabled more food to be grown for a rising global population, excessive use of these fertilizers contributes to groundwater pollution by nitrate (NO_3^-) and nitrite (NO_2^-).[2] High concentrations of NO_3^- in groundwater has consequences for human and oceanic health. Excess NO_3^- in drinking water is expensive to remediate and causes methemoglobinemia, also known as blue baby syndrome, in which red blood cells are less able to carry oxygen, resulting in increased risk of miscarriage or birth defects.[2] The Pacific Northwest coast is particularly vulnerable to groundwater-borne contamination of NO_3^-.[3] When coastal zones see an increased loading of NO_3^-, the extra source of nutrients causes algae to bloom uncontrollably.[1] When the algae die, their decomposition strips the water of oxygen, creating hypoxic, or "dead", zones. These dead zones cannot support aquatic life, destroying ecosystems and impacting economies that rely on seafood.

Denitrification is a step-wise process (Scheme 1) that converts NO_3^- to lower-oxidation state nitrogen species. In Nature, a different metalloenzyme catalyzes each step, each step requiring a certain number of protons and electrons. Synthetic systems that mimic these enzymes could convert NO_x^- to less harmful, and potentially useful compounds like nitrogen (N_2) and NH_3.

$NO_3^- \rightarrow NO_2^- \rightarrow NO \rightarrow N_2O \rightarrow N_2 \rightarrow NH_3$

Scheme 1. Denitrification of NO_3^-.

The Gilbertson group has previously accomplished reduction of NO_3^- and NO_2^- to NO using the pyridinediimine (PDI) ligand scaffold.[4,5] By incorporating different hemilabile, proton-responsive groups into the secondary coordination sphere of the ligand, the rates and yields of the reactions could be controlled. The reduction of NO_3^- to NO requires three electrons and four protons, while NO_2^- reduction requires one electron and two protons. Both reactions preferentially produce a dinitrosyl iron complex (DNIC), which is extremely stable.[4] When a hemilabile pendant amine was used in the NO_2^- reduction and the stoichiometry was controlled, a mononitrosyl iron complex (MNIC) was produced.

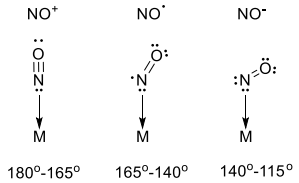

Figure 1. Binding modes of NO.

Mononitrosyl iron complexes (MNICs) are highly prevalent in biology, having such purposes as NO sensing, transport, intermediates in nitrogen-cycle enzymes, and bacterial NO reductases.[6] Metal-nitrosyl

complexes are redox non-innocent, as the NO can coordinate to the metal in any of three oxidation states, characterized by the angle of the M-N-O unit (Figure 1). The primary and secondary coordination sphere of the ligand affects Fe-NO electronics and reactivity. Hemilabile ligands, Lewis acids, and π-acceptor ligands have all been used to enhance NO_2^- reduction to NO, activate NO towards N-N coupling, or stabilize various oxidation states of the same complex.[4,7,8]

This work introduces a new PDI iron complex (Figure 2) featuring a hemilabile diphenylphosphine group in the secondary coordination sphere. Its unusual behavior and reactivity towards nitrous oxide (N_2O), NO_2^-, and NO_3^- is investigated. Experimental work is supported by DFT broken symmetry calculations.

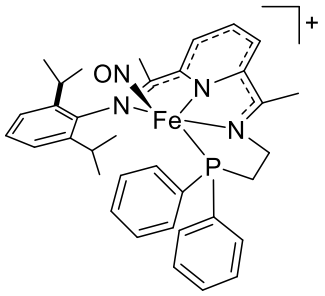

Figure 2. Hemilabile phosphine PDI Complex (100).

Experimental Section

Ligand 3. In a round-bottom flask, 2,6-diacetylpyridine (3 g, 18 mmol) was dissolved in methanol (MeOH) and placed in an ice bath. One equivalent of 2,6-diisopropylaniline (3.3 g, 18 mmol) was dissolved in MeOH and then added slowly to the 2,6-diacetylpyridine and MeOH while stirring. A catalytic amount of formic acid (0.25 mL) was added. After stirring for one hour, the flask was moved to the fridge to precipitate. The yellow precipitate was filtered through a Buchner funnel and washed with cold MeOH, yielding 5 g (85%) of Ligand 3. $\nu_{C=O}$ = 1698 cm^{-1}, $\nu_{C=N}$ = 1647 cm^{-1}.

100FeX$_2$. In a Schlenk flask in the glove box, ligand 3 (0.75 g, 2.3 mmol) and one equivalent $FeCl_2$ (0.32 g, 2.5 mmol) or $FeBr_2$ were dissolved in anhydrous EtOH. One equivalent of 2-(diphenylphosphino)ethylamine (0.59 g, 2.5 mmol) was dissolved in EtOH in a vial, which was fitted with a septum. The Schlenk flask was brought out of the glovebox and placed under a nitrogen atmosphere and heated to 40 °C while stirring. The arm was added to the reaction with a syringe. The blue solution was heated to 60 °C and stirred overnight. The solvent was evaporated and the Schlenk flask was brought into the glovebox, where the blue precipitate was redissolved in DCM. This solution was filtered through celite, concentrated, and layered with Et_2O to produce crystals suitable for XRD.

100FeCO (direduced). 100$FeCl_2$ (0.19 g, 0.29 mmol) and 2.1 equivalents of samarium(II) iodide (SmI_2) (~0.1 M in THF (13.7 mL), concentration measured by UV-Vis) were added to a side-arm Schlenk tube with a stir bar in the glovebox. Upon adding the SmI_2, the solution immediately changed from blue to dark red/brown. The headspace of the tube was evacuated and brought out of the glovebox, where it was charged with one equivalent of carbon monoxide (CO) (7 mL, 1 atm). The red solution was stirred vigorously overnight, after which it was dried and brought into the glovebox. The brown solid was redissolved in Et_2O and filtered through celite. The solution of 100FeCO was dried and redissolved in Et_2O. To purify the complex, this solution was filtered through an alumina plug, then allowed to evaporate slowly, yielding crystalline 100FeCO. It was characterized through FTIR and ^{1}H, ^{13}C, and ^{31}P NMR. ν_{CO} = 1858 cm^{-1}. ^{31}P NMR δ: 64 ppm.

100FeCO (monoreduced). 100$FeCl_2$ and 1 equivalent of samarium(II) iodide (SmI_2) (~0.1 M in THF, concentration measured by UV-Vis) were added to a Fischer Porter (FP) tube with a stir bar in the

glovebox. The FP tube was fitted with a pressure gauge and brought out of the glovebox, where it was charged with 40 psi of carbon monoxide (CO). The red solution (no immediate color change) was stirred vigorously overnight. Upon pulling a vacuum, the solution turned blue. The solution which it was dried and brought into the glovebox. The solid was dissolved in DCM and filtered through celite. This solution was concentrated and layered with Et_2O to produce crystals suitable for XRD. The paramagnetic solid was characterized through FTIR and ^{31}P NMR. ν_{CO} = 1985 cm^{-1}. ^{31}P NMR δ: 40.8 ppm.

Synthesis of 100FeCO with NaHg. $100FeCl_2$ (0.5 g, 0.76 mmol) and 2.1 equivalents of sodium mercury amalgam (NaHg) (5% Na) (0.93 g NaHg, 1.6 mmol Na) dissolved in DCM in a Fischer Porter (FP) tube with a stir bar in the glovebox. The FP tube was fitted with a pressure gauge and brought out of the glovebox, where it was charged with 40 psi of carbon monoxide (CO). The green solution was stirred vigorously for two days, during which it turned red/brown. It was dried and brought into the glovebox. The brown solid was redissolved in Et_2O and filtered through celite. Separation of products was attempted by filtering through an alumina plug, but this was unsuccessful. It was characterized through FTIR and ^{1}H, ^{13}C, and ^{31}P NMR. ν_{CO} = 1946, 1882, 1855 cm^{-1}. ^{31}P NMR δ: 64, -20 ppm.

Reaction of 100FeCO with N_2O. 100FeCO (direduced) (0.0683 g, 0.11 mmol) was dissolved in THF in a side arm flask, which was then degassed through three rounds of freeze-pump-thaw. One equivalent N_2O (2.7 mL, 1 atm) was layered onto the frozen solution. To another flask was added the same volume of THF and N_2O. Both flasks were wrapped in foil and stirred for two days at room temperature. The headspace of both flasks was sampled for GC and IR analysis.

[100FeX][BPh_4]. $100FeCl_2$ (0.1894 g, 0.29 mmol) or $100FeBr_2$ was dissolved in DCM in a scintillation vial equipped with a magnetic stir bar. Ammonium hexafluorophosphate (NH_4PF_6) (0.0476 g, 0.29 mmol) or sodium tetraphenylborate ($NaBPh_4$) (one equivalent) was dissolved in a minimal amount of MeOH and added dropwise to the dihalide complex while stirring. An immediate color change from blue to blue/purple was observed. The reaction was stirred overnight before pulling removing all solvents and redissolving in DCM. The magenta solution was filtered through a celite plug, leaving a white precipitate. This solution was layered with Et_2O, giving a solid. Using excess salt (1.5 equivalents) produced the same result.

NO_2^- Reduction. 100FeCO (direduced) (0.0771 g, 0.12 mmol) and two equivalents triethylammonium tetraphenylborate ([$HNEt_3$][BPh_4]) (0.1065 g, 0.25 mmol) were dissolved in THF in a side arm flask and stirred. Exactly one equivalent sodium nitrite ($NaNO_2$) (0.0088 g, 0.13 mmol) was dissolved in a minimal amount of MeOH and added dropwise to the reaction flask, which was then immediately sealed and allowed to stir overnight. After an hour, the color changed from red to brownish green. The headspace of the reaction was sampled for IR analysis before drying the solution *in vacuo*. The black solid was triturated in Et_2O overnight to remove unreacted 100FeCO. The red Et_2O solution was filtered through celite and the remaining solid was dissolved in DCM. The green solution was filtered through celite, leaving a white precipitate ($NaBPh_4$). The DCM solution was dried and then redissolved and refiltered to purify. The DCM solution was layered with either pentane or Et_2O to produce X-ray quality crystals. These were characterized through FTIR and ^{1}H, ^{13}C, and ^{31}P NMR and CV. $\nu_{14NO/15NO}$ = 1708/1675 cm^{-1}. ^{31}P NMR δ: 49 ppm.

NO_3^- Reduction. 100FeCO (0.05 g, 0.08 mmol), $TBANO_3$, and $[HNEt_3][BPh_4]$ at varying stoichiometries were dissolved in 5 mL THF in a pressure vial and placed in an 80 °C oil bath overnight. The color changed from red to greenish brown or green depending on the stoichiometry. Solvent was removed and the solid was triturated in Et_2O before filtering through celite. The green solid was dissolved in DCM and filtered. Layering with pentane produced a green solid with white crystals identified as $TBABPh_4$. The solid was characterized through FTIR, ^1H, and ^{31}P NMR. $\nu_{14NO/15NO}$ = 1708/1675 cm^{-1}. ^{31}P NMR δ: 49 ppm.

$[100Fe(NO)_2][BPh_4]$. 1) 100FeCO (0.1027 g, 0.17 mmol) and four equivalents $[HNEt_3][BPh_4]$ (0.2818 g, 0.67 mmol) were dissolved in THF. While stirring, two equivalents $NaNO_2$ (0.0261 g, 0.38 mmol) in MeOH were added. The solution was stirred overnight, changing from red/brown to green. 2) $[100FeNO][BPh_4]$ (0.1151 g, 0.12 mmol) and two equivalents $[HNEt_3][BPh_4]$ (0.1150 g, 0.27 mmol) were dissolved in THF. While stirring, one equivalent $NaNO_2$ (0.0180 g, 0.26 mmol) in MeOH was added. After stirring for two days, no color change was observed and no change in the IR was observed. After heating overnight, some decomposition was observed. The solid was characterized through IR, ^1H, and ^{31}P NMR. ν_{14NO} = 1708 cm^{-1}. ^{31}P NMR δ: 49 ppm.

FT-IR. IR spectra were collected on a Thermo iS10 FT-IR spectrometer. Attenuated total reflectance (ATR) IR spectra were collected on a single-bounce diamond ATR accessory at a 4 cm^{-1} resolution and 16 scans. Solution-phase IR spectra were collected in a liquid IR cell equipped with Ca_F2 windows at 2 cm^{-1} resolution and 16 scans. Gas-phase IR were collected with a Pike Technologies short-pathlength (100 mm) gas transmission cell fitted with CaF_2 windows, resolution was set to 0.5 cm^{-1} and 32 scans.

NMR. All NMR spectra were collected on a Bruker Avance III 500 MHz instrument. Spectra were referenced to the solvent signal.

Cyclic voltammetry. CV were collected with a Pine WaveNow potentiostat with a glassy carbon working electrode, a platinum wire counter electrode, and a $Ag/AgNO_3$ reference electrode. Tetrabutylammonium hexafluorophosphate was employed as a supporting electrolyte at 0.1 M. Voltammograms were collected starting at the OCP and running negative on a 10 mM solution in MeCN and were internally referenced to ferrocene (Fc/Fc+).

High Performance Ion Chromatography. Ion chromatograms were collected on an Agilent 1100 series HPLC with a simple anion column and a Waters 432 conductivity detector. Samples were dissolved in 25 mL nanopure water/minimal THF. This solution was shaken vigorously, then 0.125 mL was diluted to 5 mL in nanopure water. This solution was filtered through a 0.22 µm polypropylene membrane syringe filter into a GC vial for analysis in triplicate. Calibrations was completed using external standards made from $TBANO_3$. Ion retention times (in minutes) are as follows: NO_3^-: 3.98, Cl^-: 2.2.

UV-Visible Spectroscopy. UV-vis spectra were collected on a JASCO V-670 spectrometer at room temperature in a 1 cm quartz cuvette (Starna Cells). Samples were dissolved in 10 mL THF. Then 0.4 mL was diluted to 10 mL in THF. Spectra were collected with both a solvent baseline as well as a dark correction at a scan rate of 400 nm/min with a near-IR resolution of 4 nm and an ultraviolet-visible resolution of 2 nm, sampled every 1 nm.

Computational Methods. Broken symmetry DFT calculations were performed on 8 MNICs. CIF files were imported into WebMO and modified as needed to perform ORCA electronic structure calculations. Calculations were performed with charge +1 and multiplicity 3 on complexes. The BLYP functional and def2-SV(P) basis set were used to perform molecular energy calculations and geometry optimizations. The optimized structures were then refined using the PBE0 functional and def2-TZVP basis set with the RIJCOSX approximation. Open and closed shell NBO calculations were performed in QChem with the omegaB97X-D functional and 6-31G* basis set with multiplicity 1.

Results and Discussion

Carbonyl Compounds

The reduced monocarbonyl phosphine complex (100FeCO) was synthesized through a multistep reaction with SmI_2 as the reductant (Scheme 1).

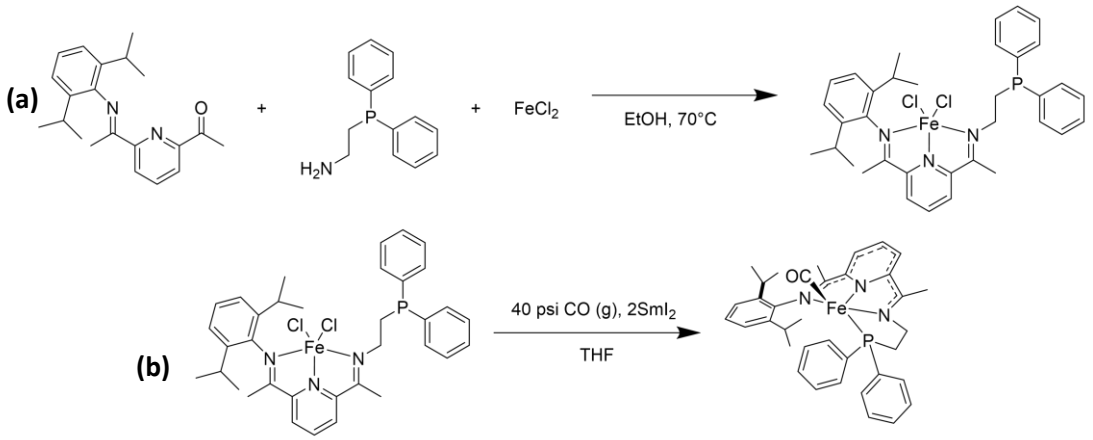

Scheme 1. (a) Synthesis of $100FeCl_2$. **(b)** Synthesis of 100FeCO.

The IR spectrum of 100FeCO (Figure 3) showed one strong band at 1858 cm^{-1}, indicating a monocarbonyl species. In contrast to previous reduced green dicarbonyls, 100FeCO is a red/brown color.

The ^{1}H NMR of 100FeCO (Figure S2) indicated that it was diamagnetic. One of the isopropyl proton peaks appeared at a negative chemical shift relative to TMS. This suggested that one of the isopropyl groups was positioned such that it was in the deshielding zone of one of the phenyl groups on the phosphine arm. The crystal structure of 100FeCO confirmed this (Figure 3b). The ^{31}P NMR of 100FeCO (Figure S4) showed one peak at 64 ppm, shifted downfield from -20.7 ppm in the free phosphine arm.[9] A downfield shift is indicative of a metal-bound phosphine.

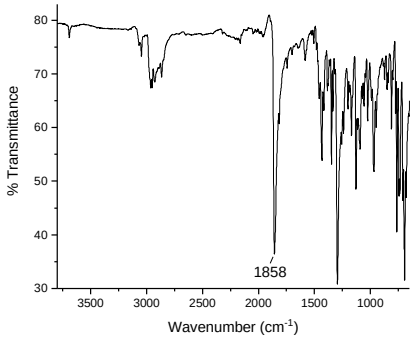

Figure 3. IR spectrum of 100FeCO. ν_{CO} = 1858 cm^{-1}.

To determine the oxidation state of 100FeCO, its crystal structure was compared to that of $100FeCl_2$ (Figure 4). A summary of bond lengths is given in Table 1. The imine bond lengths lengthened from 1.29 Å in $100FeCl_2$ to 1.34 Å in 100FeCO, and the C_{imine}-$C_{pyridine}$ bond lengths shortened from 1.489 to 1.425 Å, indicating that the PDI ligand was reduced. These bond lengths were similar to previous iron dicarbonyl PDI complexes reduced

by two electrons.[4] These data, along with the observation that 100FeCO is diamagnetic, suggest that this complex has been reduced by two electrons and is a low spin Fe(II) center.

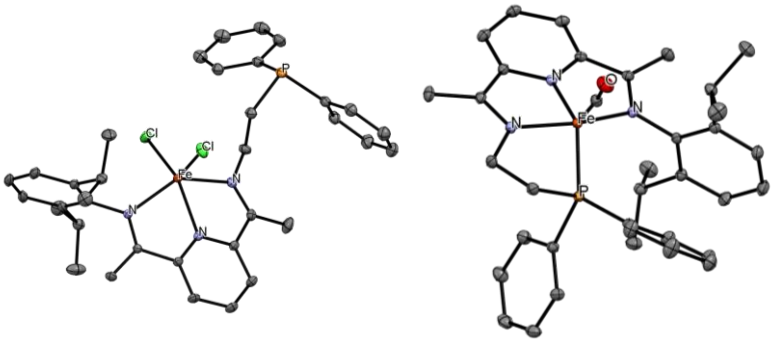

Figure 4. (left) Crystal structure of 100FeCl$_2$. **(right)** Crystal structure of 100FeCO.

A one electron-reduced monocarbonyl was also synthesized using one equivalent SmI_2. This blue species was paramagnetic, and the CO stretch appeared at 1985 cm^{-1} (Figure S6). The color of the reaction solution changed from red to blue upon pulling vacuum, indicating the CO was labile. This is consistent with a higher IR stretching frequency. The phosphine appeared at 41 ppm in the ^{31}P NMR spectrum (Figure S7), upfield of the direduced monocarbonyl. However, upon crystallization, the CO IR stretch disappeared, and the crystal structure showed that the phosphorous was not coordinated. It is still unclear what the coordination sphere around the iron atom is in this complex.

When NaHg was used as the reductant, a mixture of di- and monocarbonyl, with 100Fe(CO)$_2$ being the major component, was produced. The IR spectrum showed three CO stretches at 1946, 1882, and 1854 cm^{-1} (Figure S8). The two higher wavenumber peaks are consistent with previous FePDI(CO)$_2$ complexes, while the lower peak matches the stretching frequency of 100FeCO. The ^{31}P NMR of this product mixture (Figure S9) showed a small peak at 64 ppm and a larger peak at -20 ppm, consistent with a free phosphine. Attempts to separate the two products were unsuccessful. This result shows that depending on which reductant is used, the coordination of CO to the complex can be controlled. It was found computationally that the 100FeCO + CO system is lower in energy than the 100Fe(CO)$_2$ complex by 219 kcal/mol.

CV was performed on 100FeCO to investigate its redox activity. The CV of 100FeCO in MeCN (Figure 5) shows two pseudo-reversible events, as well as other smaller events due to 100Fe(CO)$_2$ contamination. Oxidizing the complex at ~0.25 V vs $AgNO_3$ results in the IR spectrum in Figure 6. The CO stretch at 1858 cm^{-1} disappears, acomanied by the appearance of a new CO stretch at 2025 cm^{-1}. In the OTTLE cell, the reduction at -2.5 V vs $AgNO_3$ is irreversible, resulting in decomposition of the complex.

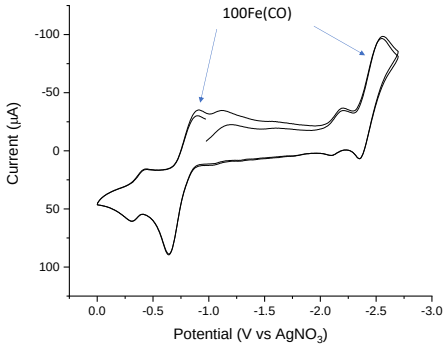

Figure 5. CV of 100FeCO in MeCN.

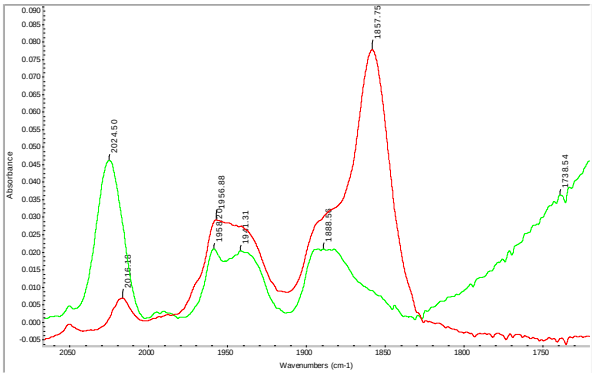

Figure 6. FT-IR of the oxidation of 100FeCO. Red = 100FeCO, green = oxidized species.

N_2O Reduction

To probe its reactivity, 100FeCO was reacted with N_2O. After 2 days, there was no color change. Analysis of the headspace by GC and IR (Figures S10 and S11) indicated that no N_2O was consumed and there were no gaseous products. A small amount of CO was observed in the IR spectrum, possibly indicating decomposition. The solid IR of the reaction (Figure S12) showed that only 100FeCO starting material was present.

NO_2^- Reduction and MNIC Formation

The MNIC of 100 was synthesized via NO_2^- reduction (Scheme 2).

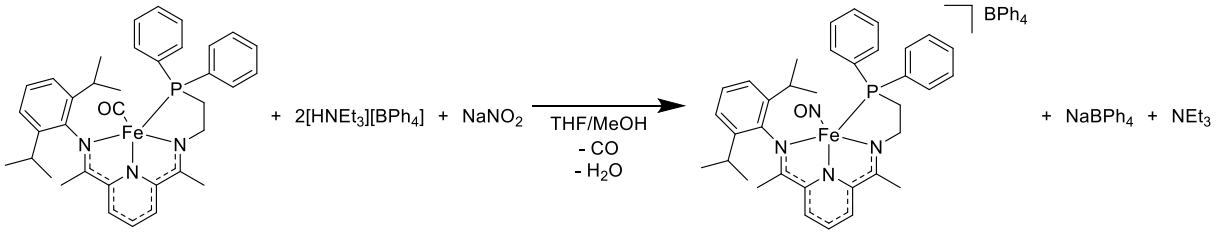

Scheme 2. Synthesis of [100FeNO][BPh_4].

The headspace of the reaction was analyzed by IR (Figure S13) to see if any gaseous products were formed. While no nitrogen species were observed, CO was present, indicating CO loss from 100FeCO. The IR spectrum (Figure 7) indicated that a mononitrosyl species was produced. The NO stretching frequency was higher than previous MNICs synthesized by the Gilbertson group, which were in the 1660-1690 cm^{-1} region.[4] This suggested that the Fe-N-O angle was more linear than previously observed.

The DNIC of 100 was attempted to be synthesized (Scheme 3) from both 100FeCO and [100FeNO][BPh_4] via NO_2^- reduction.

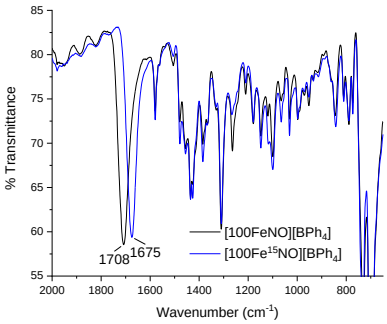

Figure 7. IR of [100FeNO][BPh_4]. $\nu_{14NO/15NO}$ = 1708/1675 cm^{-1}

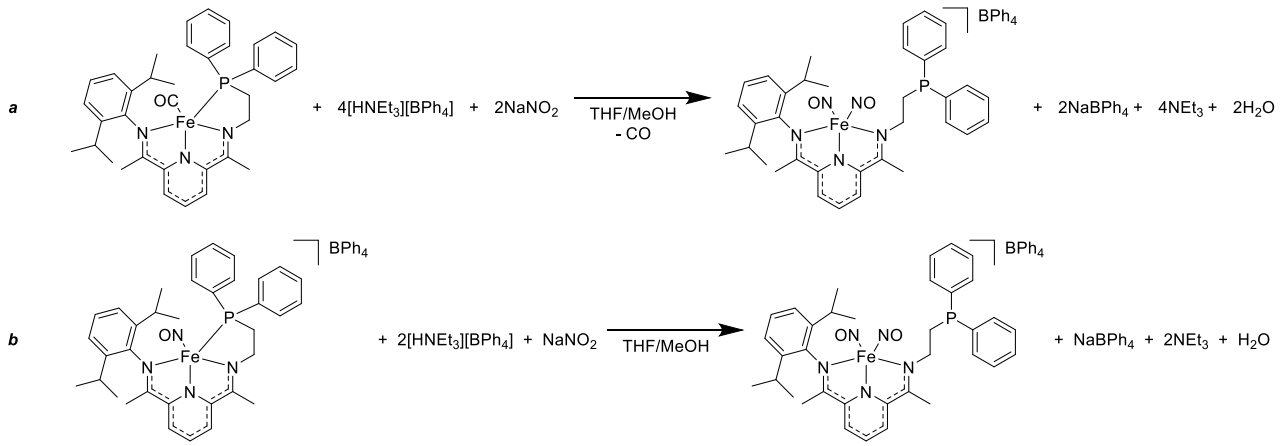

Scheme 3. Synthesis of [100Fe(NO)$_2$[BPh$_4$] from ***a)*** 100FeCO and ***b)*** [100FeNO][BPh$_4$].

Both these routes did not result in DNIC being formed (Figure 8). Heating the MNIC + NO_2^- reaction to try to initiate it only resulted in decomposition of the PDI ligand.

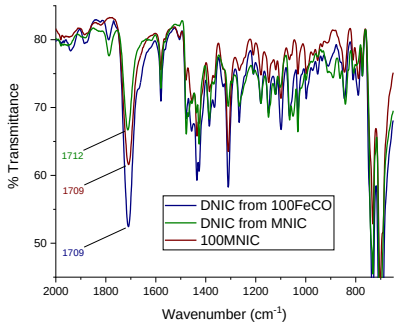

Figure 8. DNIC Syntheses showing only MNIC.

Not being able to make the DNIC from this complex is unusual, given that in other PDI complexes, the MNIC is an intermediate to the DNIC in NO_2^- reduction, and the DNIC is extremely thermodynamically stable.[4] This suggests that the Fe-P bond is very strong, enabling the MNIC to be more stable in this case.

The ^{31}P NMR of [100FeNO][BPh$_4$] (Figure S15) showed one peak at 49 ppm, shifted upfield from the 100FeCO starting material, indicating that while the phosphine was still bound to the iron center, it became more shielded.

The crystal structure of [100FeNO][BPh$_4$] (Figure 9) showed disorder in the hemilabile phosphine arm as well as the nitrosyl oxygen. The Fe-N-O unit was more linear 78% of the time and more bent 22% of the time. A summary of bond angles and lengths compared to 100FeCO as well as previous MNICs is given in Table 1.

In the major case, the Fe-N-O angle was 169.53°, much more linear than in other MNICs. The imine bond lengths shortened slightly from 100FeCO and the C_{imine}-$C_{pyridine}$ bond lengths lengthened slightly. This indicates that the PDI is still reduced in the MNIC, but not as much as the carbonyl. The PDI bond lengths in the MNIC were comparable to those of the other MNICs.

Previous MNICs contained hemilabile N-donors, while 100 contains a P-donor. Phosphines are softer ligands and interact differently with the d-orbitals on the metal. This interaction could be enabling the more linear Fe-N-O unit and could influence the reactivity of the MNIC.

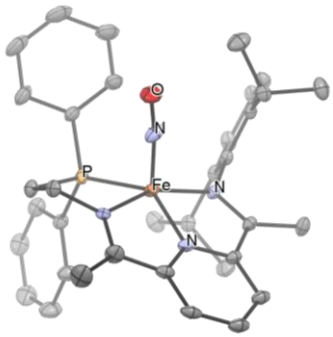

Figure 9. Crystal structure of [100FeNO][BPh$_4$]. H atoms and BPh_4^- omitted for clarity.

Table 1. Bond lengths (Å) and angles of crystal structures.

	100FeCl$_2$	**100FeCO**	**[100FeNO][BPh$_4$]**	**[44FeNO][BPh$_4$]**	**[41FeNO][BPh$_4$]**
N-O IR stretch			1708 cm^{-1}	1667 cm^{-1}	1687 cm^{-1}
Fe-N-O		174.3° (Fe-C-O)	169.53°(78%) 141.30 (22%)	150.85°	154.40°
Fe-N(O)			1.666	1.677	1.679
N-O			1.204/1.163	1.182	1.183
Fe-N$_{imine}$	2.217	1.923	2.024	1.894	1.894
	2.248	1.963	2.038/1.922	2.031	2.035
Fe-N$_{pyridine}$	2.089	1.838	1.860	1.830	1.836
N$_{imine}$-C	1.288	1.332	1.439/1.314	1.313	1.313
	1.289	1.344	1.314	1.315	1.314
C$_{imine}$-C$_{pyridine}$	1.489	1.426	1.435	1.439	1.440
	1.488	1.424	1.447	1.453	1.446

To further investigate the electronics of the MNIC, cyclic voltammetry was performed. The open circuit potential of the complex was -0.548 V vs Fc. The CV (Figures S17 and S18) displayed three redox events, one reversible event centered at -1.52 V vs Fc and two irreversible events at -0.05 V vs Fc and -2.16 V vs Fc. The presence of the reversible event suggest that the complex could be chemically reduced by one electron. This was investigated in the OTTLE cell (Figures 10 and 11). The starting complex (in blue) can undergo a reversible one-electron reduction to form the neutral complex (purple) as well as an irreversible one electron oxidation. The oxidation (red) appears to form a DNIC based on the ν_{NO} at 1850 and 1800 cm^{-1}, however the $\Delta\nu_{NO}$ is rather small for the expected square pyramidal {Fe(NO)$_2$}^{9} complex and appears to be more in line with a tetrahedral DNIC. The small reduction at 0.25 V is likely due to side products forming after oxidation.

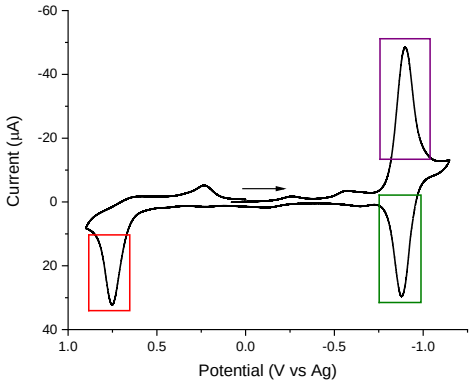

Figure 10. CV of [100FeNO][BPh$_4$] in MeCN.

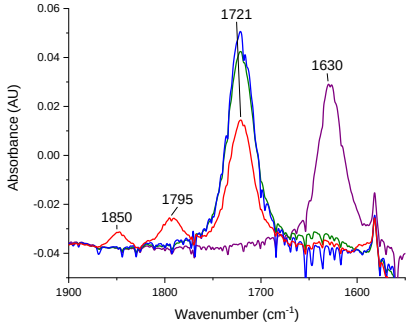

Figure 11. FT-IR of the oxidation of [100FeNO][BPh$_4$]. Colors correspond to redox events in Figure 10.

The oxidation states of the PDI, iron, and nitrosyl of the MNIC are currently unclear. The complex is diamagnetic, positively charged, and linear, with a reduced PDI. The linearity would suggest that the NO is in the +1 oxidation state. If this were the case, the PDI could be singly reduced, and the Fe would have to be Fe(I). However, the diamagnetism of the complex suggests this is not the case. More investigation is required to elucidate the electronic structure of the MNIC.

NO_3^- Reduction

To further investigate the reactivity of 100FeCO, it was reacted with a soluble nitrate source (Scheme 4).

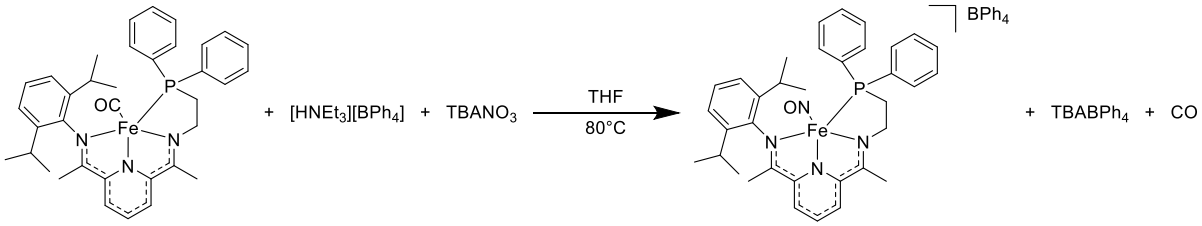

Scheme 4. Nitrate reduction with 100FeCO.

Unlike in previous experiments, no evidence of DNIC formation was observed, only MNIC (Figure 12).

Nitrate reduction to NO requires three electrons and four protons. Each 100FeCO is doubly reduced and could donate either one or two electrons. If two electrons are donated, then to reduce all of the NO_3^- to NO, a ratio of 1.5:1 100FeCO:NO_3^- would be required. If one electron is donated, then a 3:1 ratio would be required. Four equivalents of acid would be required to provide the necessary protons.

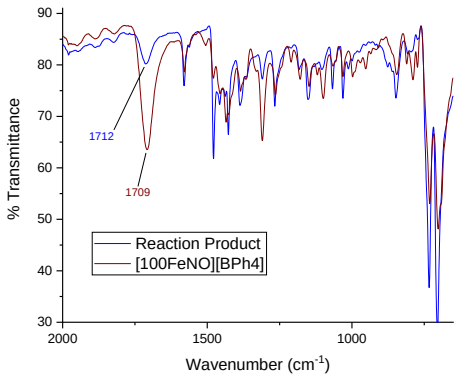

Figure 12. ATR-IR of NO_3^- reduction product. $\nu_{NO} \approx 1710\ cm^{-1}$.

Reactions with each of these ratios were performed, and a color change from red to green was observed. The liquid IRs (Figure 13) were analyzed to qualitatively determine how much 100FeCO was consumed and how much MNIC was produced. These reactions were run at the same 100FeCO concentration. It appears that about the same amount of MNIC was produced despite the 3:1 reaction starting with half the amount of NO_3^-. This was confirmed by measuring the absorbance at 594 nm of MNIC produced in these reactions *via* UV-Vis to quantify the amount of MNIC produced (Figure 14).

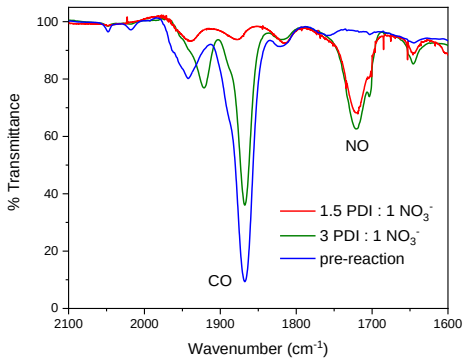

Figure 13. Liquid IRs of NO_3^- reduction reaction mixtures.

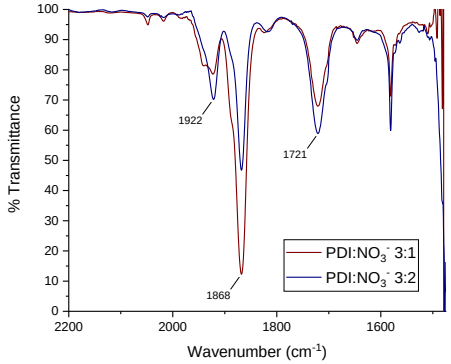

Figure 14. UV-Vis spectra of NO_3^- reduction reaction mixtures.

To measure the amount of nitrate consumed in the reaction, HPIC was performed on the reaction mixtures. The ion chromatographs (Figure 15) clearly showed that more NO_3^- was consumed in the 3:1 reaction.

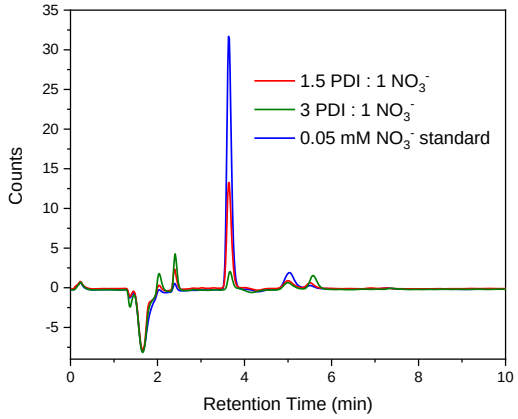

Figure 15. Ion chromatographs of NO_3^- reduction reaction mixtures. NO_3^- standard represents starting concentration of 1.5:1 reaction.

Table 2 gives a summary of the yields for the NO_3^- rediction reactions measured by UV-Vis and HPIC. The two methods were in good agreement for the amount of NO_3^- consumed and the yield of MNIC with respect to NO_3^-. Given these results, it can be concluded that the PDI donates one electron for the reduction of NO_3^- to NO. This gives more support to the conclusion that in the MNIC, the PDI backbone is reduced by one electron.

Table 2. Reaction Yields of NO_3^- Reduction Reactions.

100FeCO : NO_3^-	e^- Donated by PDI	% yield MNIC with respect to NO_3^- [a]	% yield MNIC with respect to 100FeCO [a]	% NO_3^- consumed [b]
1.5	2	60.6	40.7	57.8
3	1	112	39.5	89.6

[a] calculated from UV-Vis. [b] calculated from IC.

CONTROLS

Isotopic Labeling. NO_3^- reduction with labeled $TBA^{15}NO_3$ (Scheme 5) produced the labeled MNIC with the characteristic IR shifts (Figure S20). It also shows the possible presence of a second nitrogen species at 1922 cm^{-1} that may be hidden in the shoulder of the 1888 cm^{-1} peak in the labeled species. This could be DNIC.

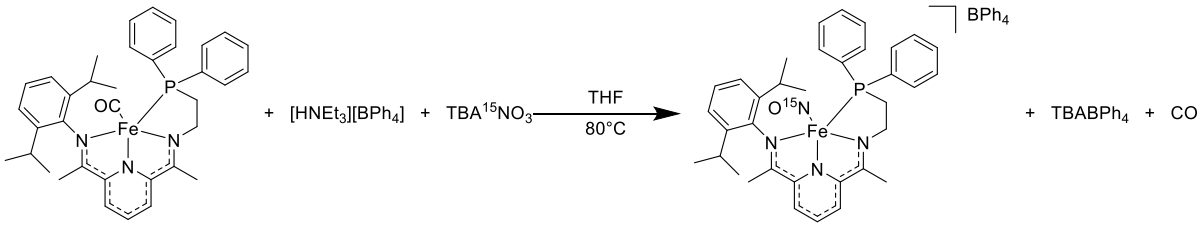

Scheme 5. Labeled nitrate reduction control.

No Heating. After stirring 100FeCO, $TBANO_3$, and $[HNEt_3][BPh_4]$ in THF at room temperature overnight (3:2:8 PDI:NO_3^-:acid) (Scheme 6), there was no evidence of a reaction. The IR was unchanged and red and white solids remained.

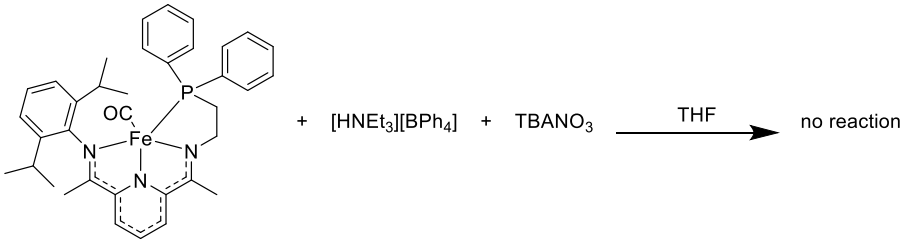

Scheme 6. Room temperature nitrate reduction.

No Nitrate. Heating 100FeCO and $[HNEt_3][BPh_4]$ in a 3:8 ratio in THF overnight (Scheme 7) resulted in no color change and no reduction in the 100FeCO IR stretch, indicating that no reaction occurred (Figure S27). This experiment wil be repeated to verify the result.

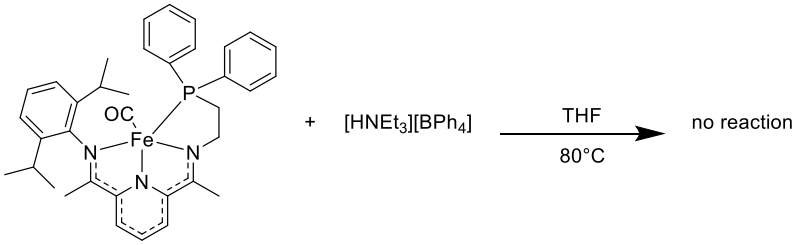

Scheme 7. Reaction of 100FeCO with $[HNEt_3][BPh_4]$.

HPIC. To determine that NO_3^- could be reliably detected, $100FeCl_2$ and $TBANO_3$ (3:8) were stirred in THF. HPIC detected 84.2% of the NO_3^- from this reaction (Figure S26).

Computational Results

In order to investigate the electronic structure of various MNICs (Figure 16), DFT geometry optimizations were performed. A summary of the important parameters (Fe-N-O angle, N-O length, Mulliken spins) is given in Table 3.

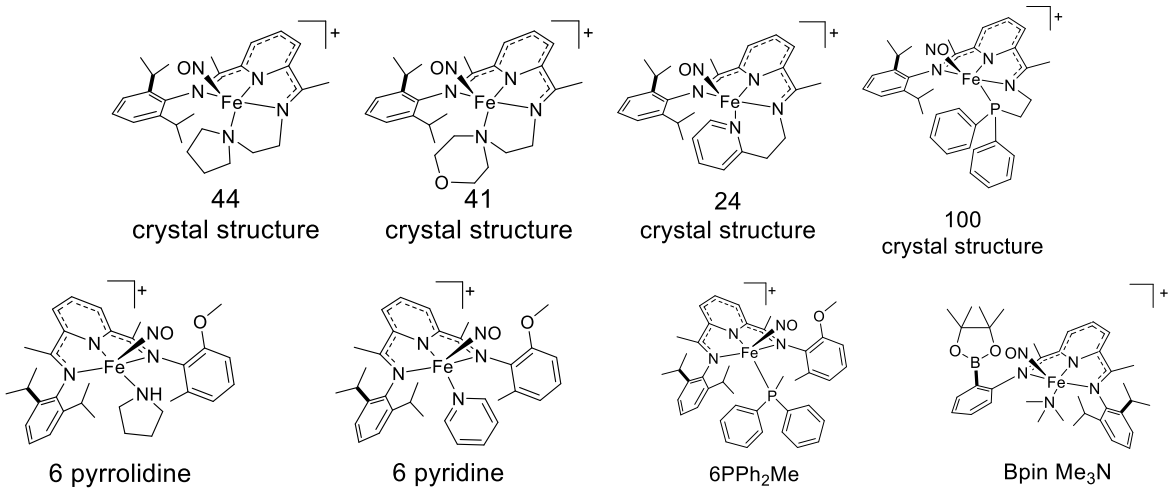

Figure 16. MNICs investigated computationally.

Table 3. Geometry Optimization Results

	44	41	24	100	6PPh_2Me (BLYP)	6 pyrrolidine	6 pyridine	Bpin Me_3N
Fe-N-O Angle	147.256°	151.439°	150.180°	155.510°	152.888°	146.639°	144.223°	156.94°
N-O Length (Å)	1.167	1.166	1.165	1.161	1.187	1.167	1.167	1.163
Mulliken Spin N	0.607	0.608	0.607	0.573		0.621	0.589	0.628
Mulliken Spin O	0.531	0.534	0.534	0.492		0.534	0.515	0.533

The results for the 44 MNIC are in good agreement with those previously published.[4] The Fe-N-O angles of 44, 41, and 24 are all in relatively good agreement with experimental data, however 100 is much less in alignment. None of the complexes vary too much in their spin populations or N-O lengths, indicating that there may not be much variation in the electronics of the FeNO unit.

Natural bond orbital calculations were performed on $[100FeNO]^+$ to examine the orbital energies and character on the Fe center, hemilabile phosphine, and NO unit. Table 4 gives the calculated natural charges and spin densities for selected atoms.

Table 4. Natural Chages and Spin Densities in $[100FeNO]^+$.

Atom	Natural Charge	Natural Spin Density
Fe	1.33005	1.87445
P	0.89996	-0.02201
N(O)	-0.12196	-0.58058
(N)O	-0.21134	-0.54015

Fe had a charge of +1 and the NO unit had a partial negative charge on it. Table 5 gives the calculated alpha and beta orbitals.

Table 5. Computed alpha and beta orbitals in $[100FeNOI]^+$.

Alpha Orbitals	Occupancy	% N Character	% O Character
N-O bonding	0.99856	39.7	60.3
N-O bonding	0.99842	40	60
N-O bonding	0.99617	42.29	57.71
N-O anti-bonding	0.07842	60.3	39.7
N-O anti-bonding	0.07066	60	40
N-O anti-bonding	0.01012	57.71	42.29
Beta Orbitals	**Occupancy**	**% Fe Character**	**% N Character**
Fe-N(O) bonding	0.97581	25.64	74.36
Fe-N(O) bonding	0.9644	28.38	71.62
Fe-N(O) anti-bonding	0.11318	74.36	25.64
Fe-N(O) anti-bonding	0.13979	71.62	28.38
		% N Character	% O Character
N-O bonding	0.99449	42.83	57.17
N-O anti-bonding	0.00412	57.17	42.83

There were three spin up N-O bonding and three anti-bonding orbitalsorbitals, corresponding to three electrons. There was only one spin down N-O bonding and one anti-bonding orbital, corresponding to one electron. There were no spin-up Fe-N bonds, but there were two spin down bonding and two anti-bonding orbitals, corresponding to two electrons. There were no Fe-P bonds listed, suggesting that the Fe and the hemilabile phosphine are not interacting with each other in the complex.

Conclusions

A new and unusual PDI complex with a hemilabile phosphine in the secondary coordination sphere was synthesized and characterized. On this ligand scaffold, both NO3- and NO2- are selectively reduced to NO in the form of an MNIC, with no DNIC being formed. Until now, the DNIC has been the thermodynamic product that prevents us from moving down the nitrogen cycle past nitric oxide. MNICs are historically much more reactive than DNICs, and for example facilitating N-N coupling to produce N_2O. Incorporating the phosphine arm has solved this problem by eliminating the DNIC.

Future work on this project will indclude fully characterizing the electronic structure of the MNIC and investigating its reactivity.

Computationally, eight MNICs with different basal ligands were investigated and geometries and electronics characterized. Natural bond orbital calculations were performed and analzyed on $[100FeNO]^+$.

References

(1) Fields, S. Global Nitrogen: Cycling out of Control. *Environ. Health Perspect.* **2004**, *112* (10), 556–563.

(2) Morgan, L. *Washington Nitrate Prioritization Project*; 16-10–011; Washington State Department of Ecology, 2016; p 102.

(3) Sawyer, A. H.; David, C. H.; Famiglietti, J. S. Continental Patterns of Submarine Groundwater Discharge Reveal Coastal Vulnerabilities. *Science* **2016**, *353* (6300), 705–707. https://doi.org/10.1126/science.aag1058.

(4) Cheung, P. M.; Burns, K.; Kwon, Y.; Deshaye, M.; Aguayo, K.; Oswald, V.; Seda, T.; Zakharov, L.; Kowalczyk, T.; Gilbertson, J. Hemilabile Proton Relays and Redox Activity Lead to $\{FeNO\}^x$ and Significant Rate Enhancements in NO_2^- Reduction. *J. Am. Chem. Soc.* **2018**, *140* (49), 17040–17050. https://doi.org/10.1021/jacs.8b08520.

(5) Delgado, M.; Gilbertson, J. D. Ligand-Based Reduction of Nitrate to Nitric Oxide Utilizing a Proton-Responsive Secondary Coordination Sphere. *Chem Commun* **2017**, *53* (81), 11249–11252. https://doi.org/10.1039/C7CC06541H.

(6) Dong, H. T.; Chalkley, M. J.; Oyala, P. H.; Zhao, J.; Alp, E. E.; Hu, M. Y.; Peters, J. C.; Lehnert, N. Exploring the Limits of Dative Boratrane Bonding: Iron as a Strong Lewis Base in Low-Valent Non-Heme Iron-Nitrosyl Complexes. *Inorg. Chem.* **2020**, *59* (20), 14967–14982. https://doi.org/10.1021/acs.inorgchem.0c01686.

(7) Abucayon, E.; Khade, R.; Powell, D.; Zhang, Y.; Richter-Addo, G. Lewis Acid Activation of the Ferrous Heme–NO Fragment toward the N–N Coupling Reaction with NO To Generate N_2O. *J. Am. Chem. Soc.* **2018**, *140*, 4204–4207. https://doi.org/10.1021/jacs.7b13681.

(8) Chalkley, M. J.; Peters, J. C. A Triad of Highly Reduced, Linear Iron Nitrosyl Complexes: $\{FeNO\}^{8–10}$. *Angew. Chem. Int. Ed.* **2016**, *55* (39), 11995–11998. https://doi.org/10.1002/anie.201605403.

(9) Jia, W.; Chen, X.; Guo, R.; Sui-Seng, C.; Amoroso, D.; Lough, A. J.; Abdur-Rashid, K. Aminophosphine Ligands $R_2P(CH_2)_nNH_2$ and Ruthenium Hydrogenation Catalysts $RuCl_2(R_2P(CH_2)_nNH_2)_2$. *Dalton Trans.* **2009**, No. 39, 8301. https://doi.org/10.1039/b911459a.

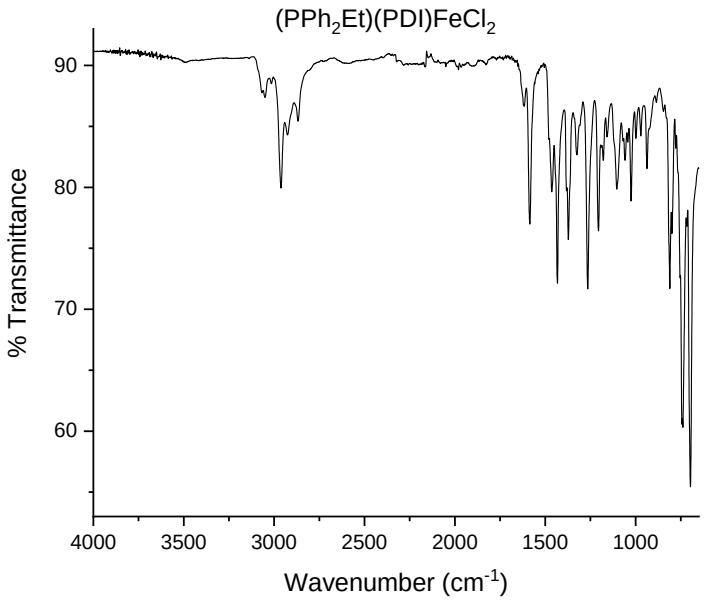

Figure S1. FT-IR Spectrum of 100$FeCl_2$.

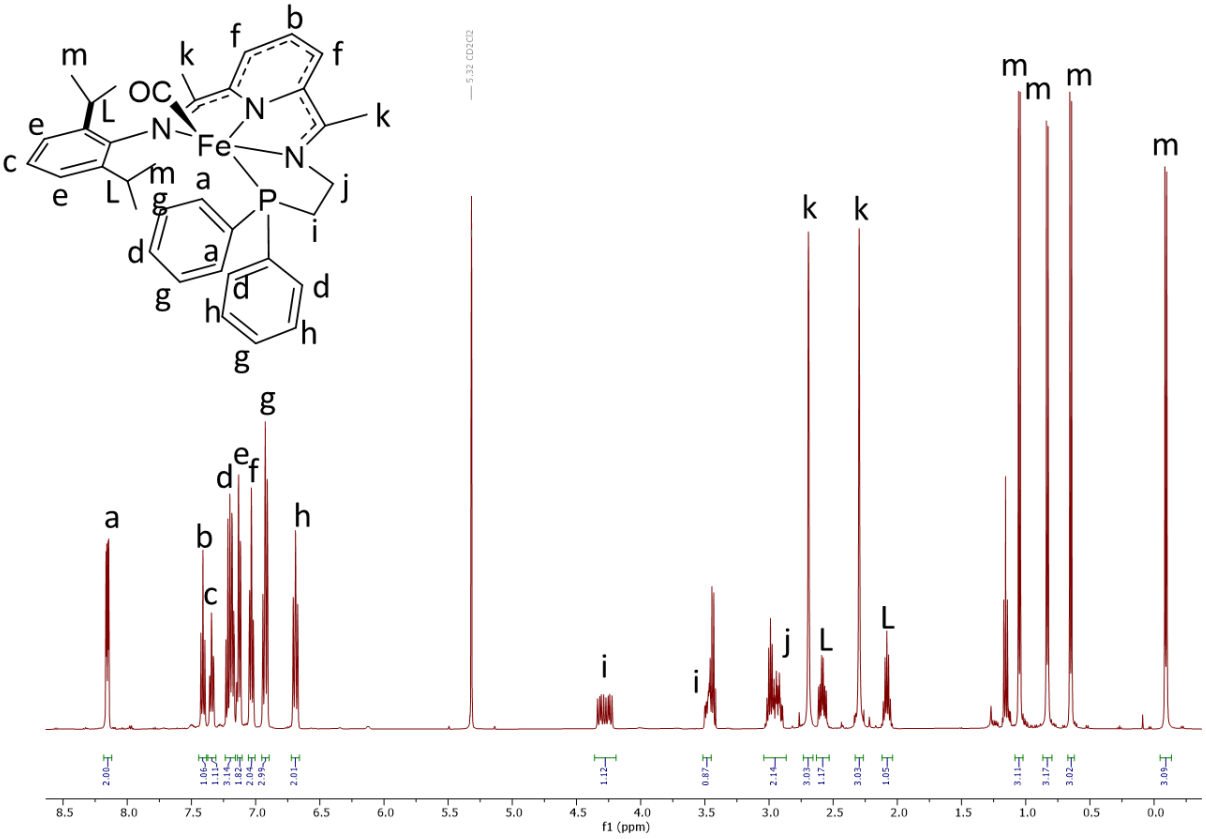

Figure S2. ^{1}H NMR Spectrum of 100FeCO.

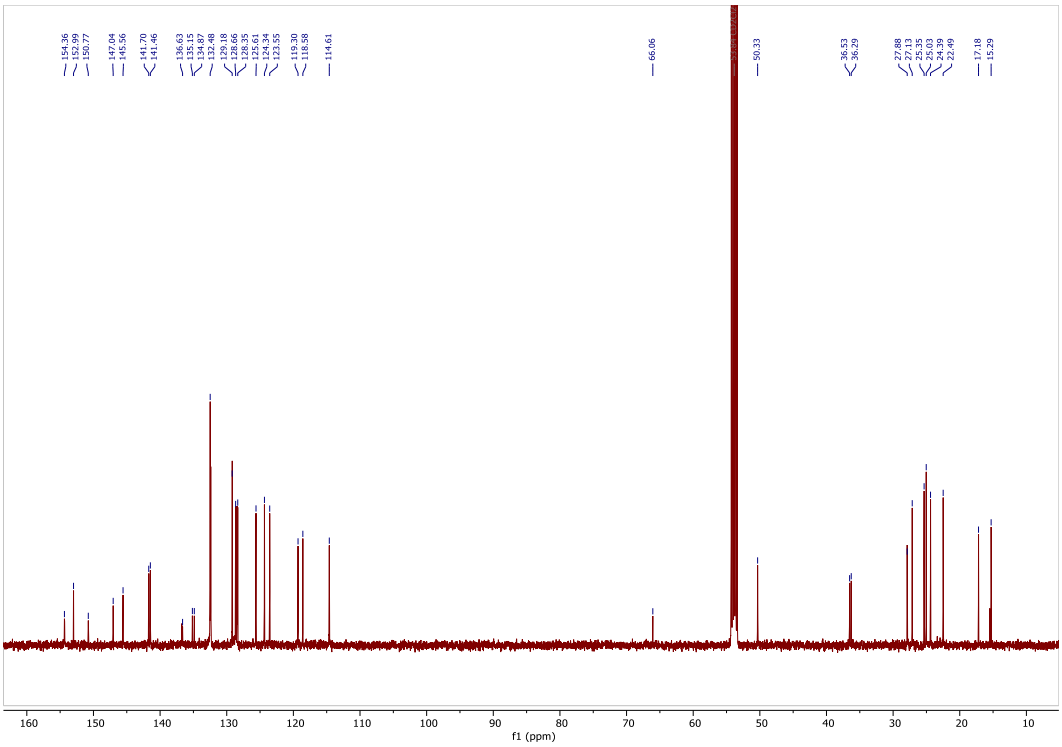

Figure S3. ^{13}C NMR Spectrum of 100FeCO.

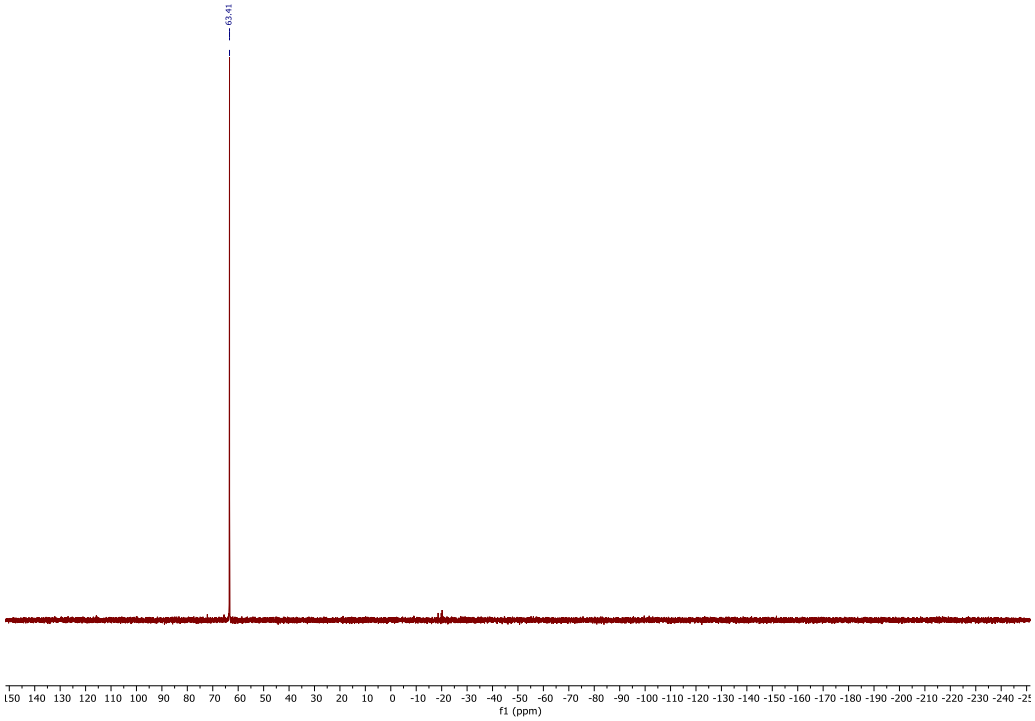

Figure S4. ^{31}P NMR Spectrum of 100FeCO.

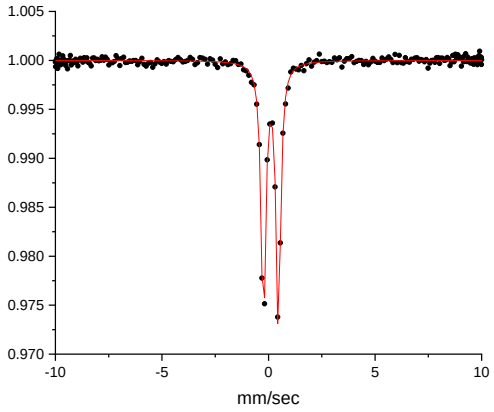

Figure S5. Mossbauer spectrum of 100FeCO. Isomershift, δ: 0.213(1) mm/s. Quadrupole splitting, ΔE_Q: 0.704(2) mm/s. Line width, Γ: 0.251(3) mm/s.

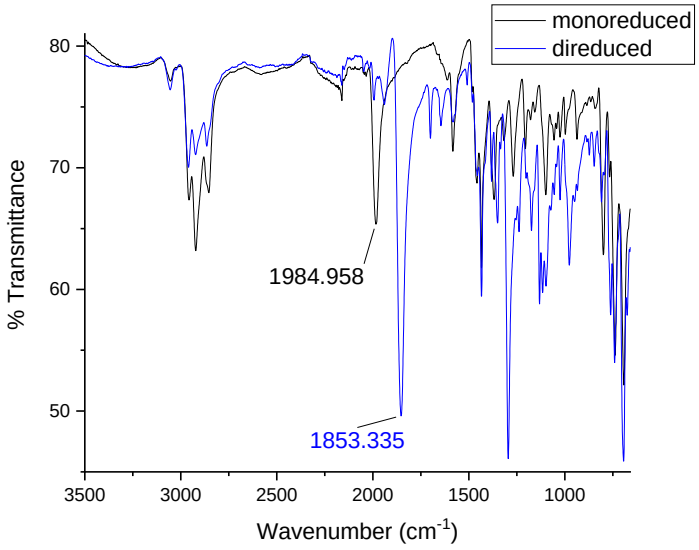

Figure S6. FT-IR spectra of mono- (black) and direduced (blue) 100FeCO species.

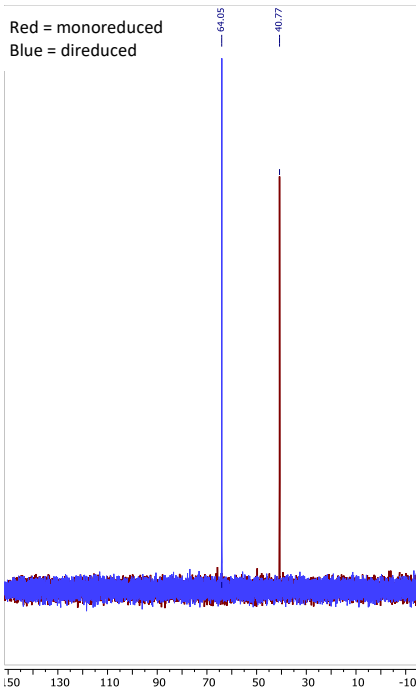

Figure S7. ^{31}P NMR spectra of mono- (red) and direduced (blue) 100FeCO species.

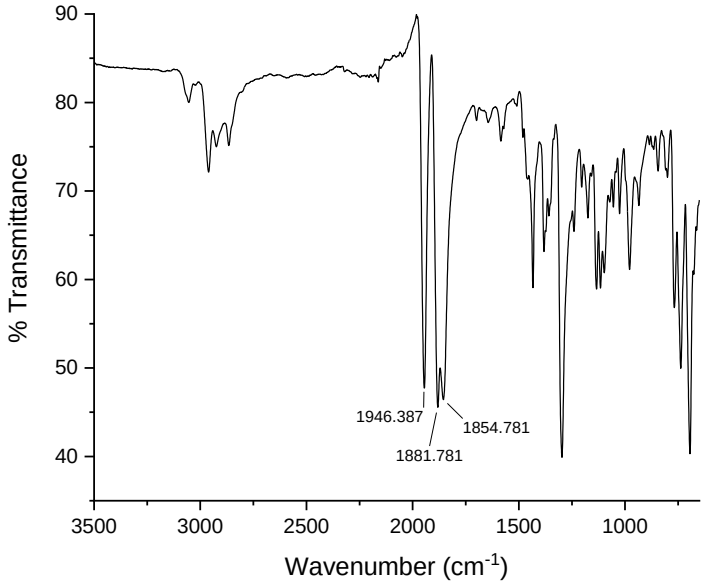

Figure S8. FT-IR spectrum of mixture of 100FeCO and 100$Fe(CO)_2$.

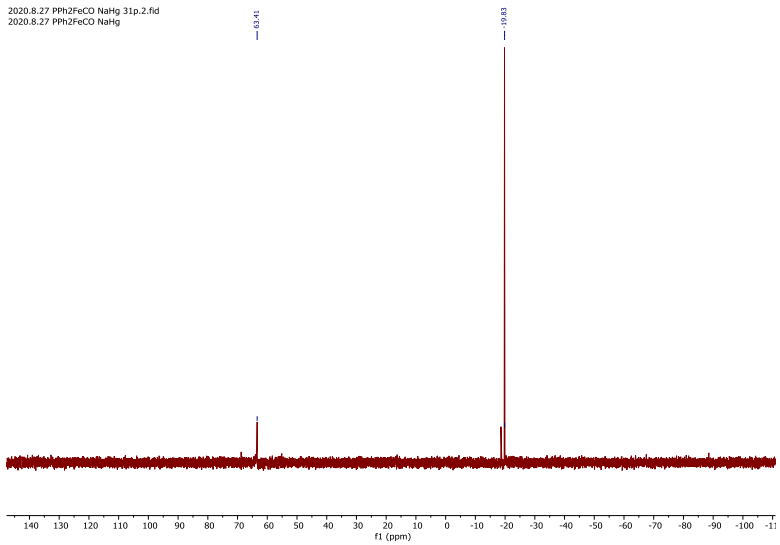

Figure S9. ^{31}P NMR spectrum of mixture of 100FeCO and 100$Fe(CO)_2$.

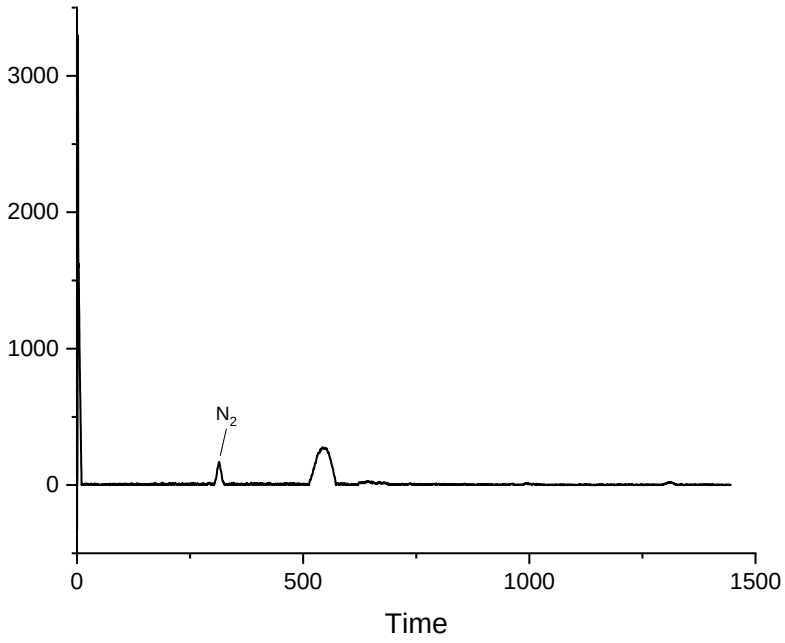

Figure S10. GC of 100FeCO + N_2O reaction headspace after stirring for 2 days.

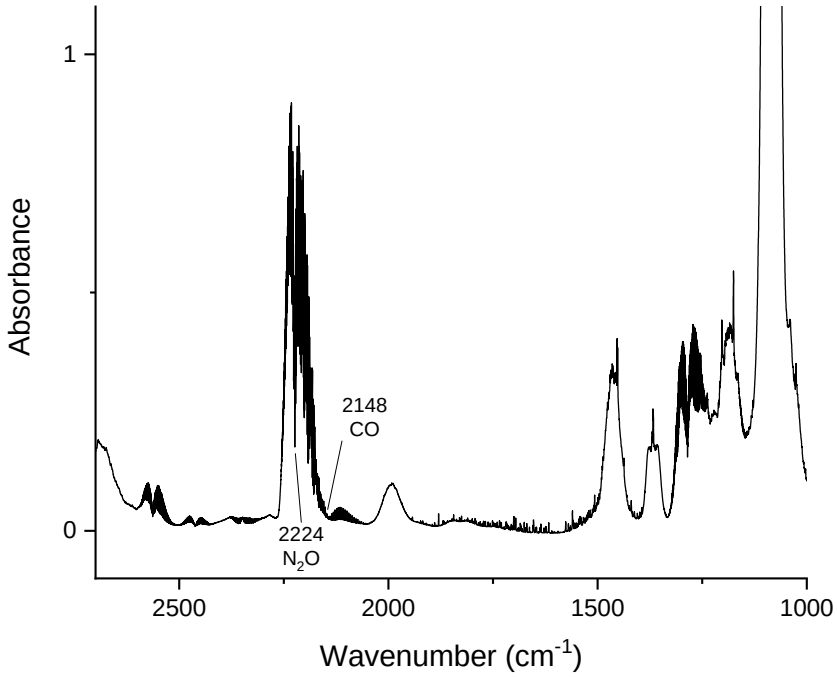

Figure S11. FT-IR spectrum of 100FeCO + N_2O reaction headspace after stirring for 2 days.

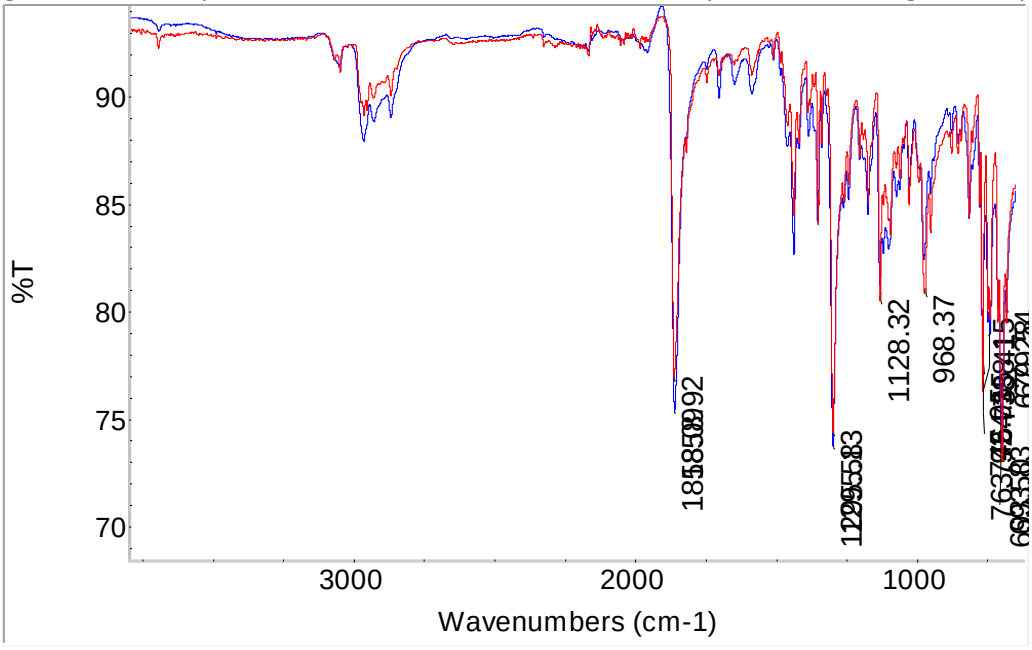

Figure S12. FT-IR spectra of 100FeCO + N_2O reaction solid (blue) and 100FeCO (red).

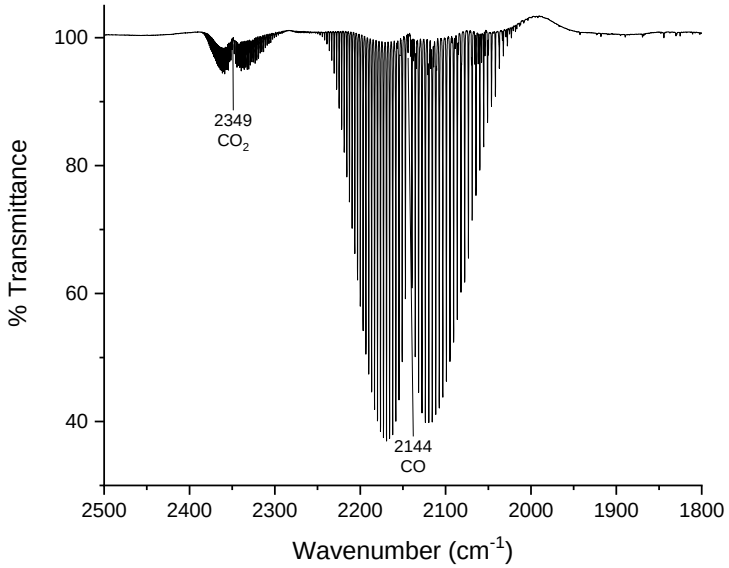

Figure S13. FT-IR spectrum of NO_2^- reduction reaction headspace.

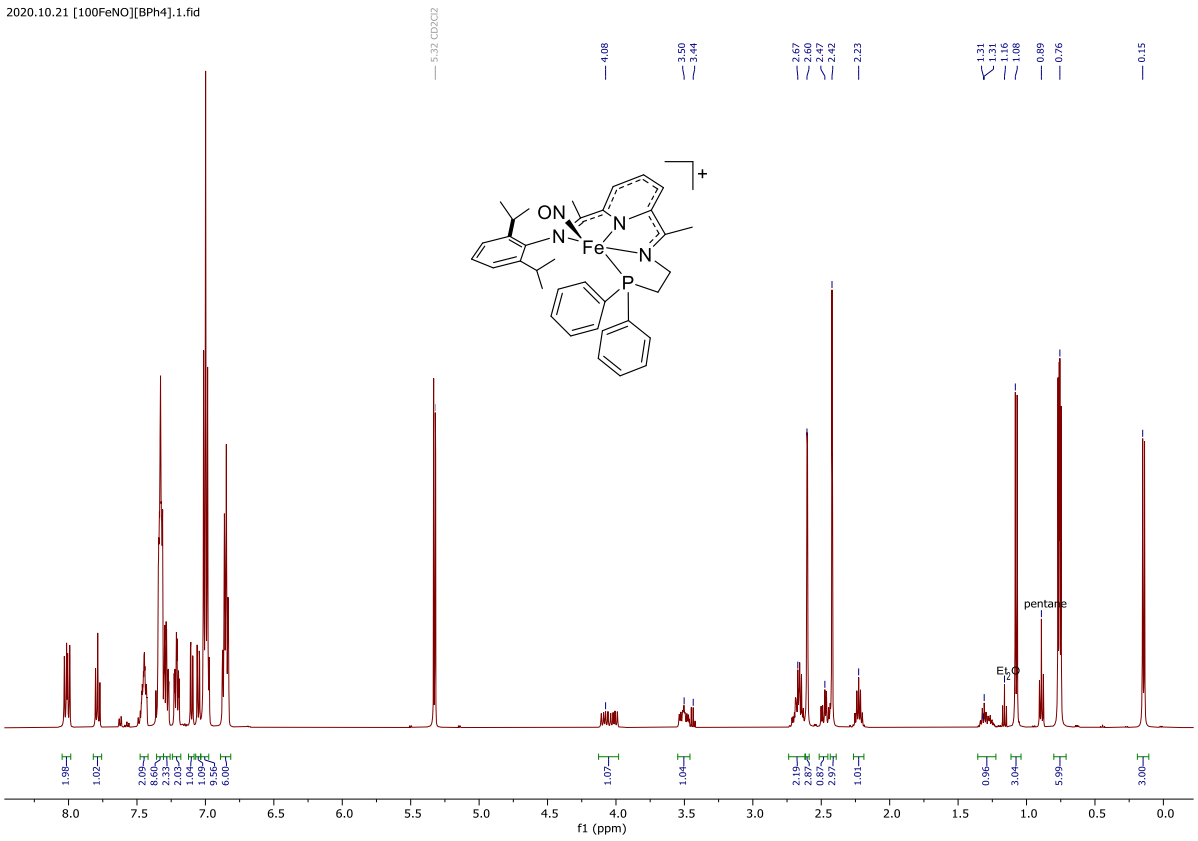

Figure S14. ^{1}H NMR spectrum of [100FeNO][BPh_4].

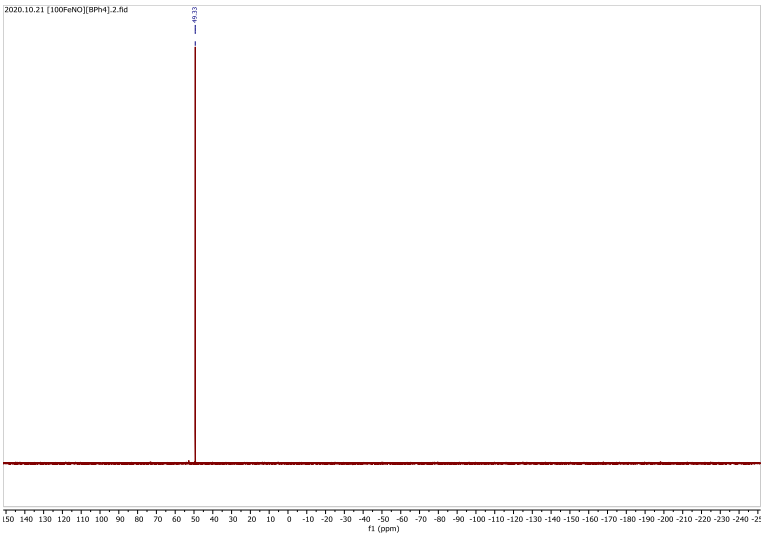

Figure S15. ^{31}P NMR spectrum of [100FeNO][BPh_4].

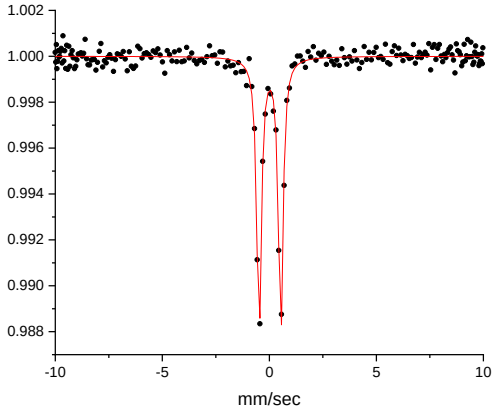

Figure S16. Mossbauer spectrum of [100FeNO][BPh_4]. Isomershift, δ: 0.127(2) mm/s. Quadrupole splitting, ΔE_Q: 1.012(6) mm/s. Line width, Γ: 0.255(7) mm/s.

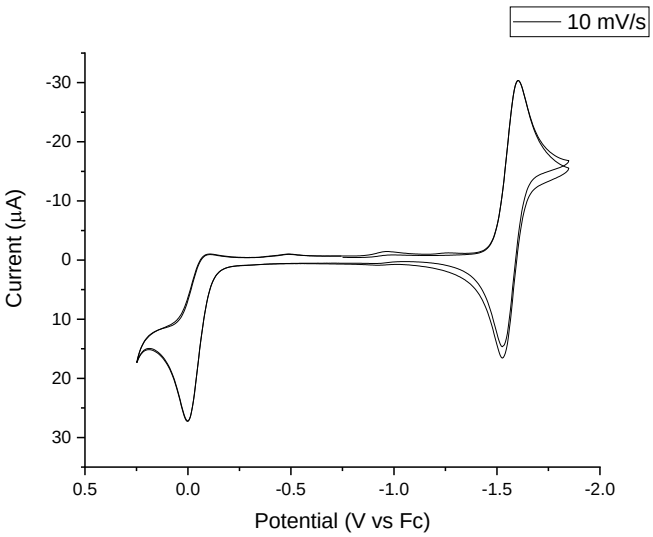

Figure S17. Cyclic voltammogram of [100FeNO][BPh_4].

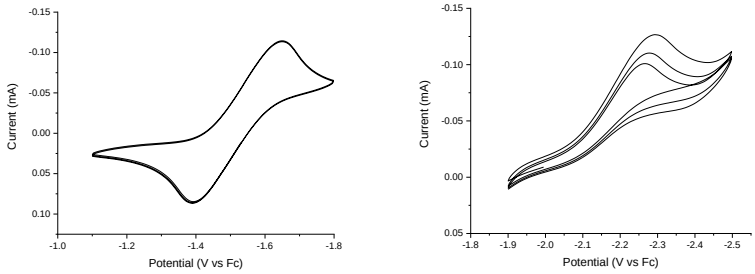

Figure S18. Cyclic voltammograms of [100FeNO][BPh_4].

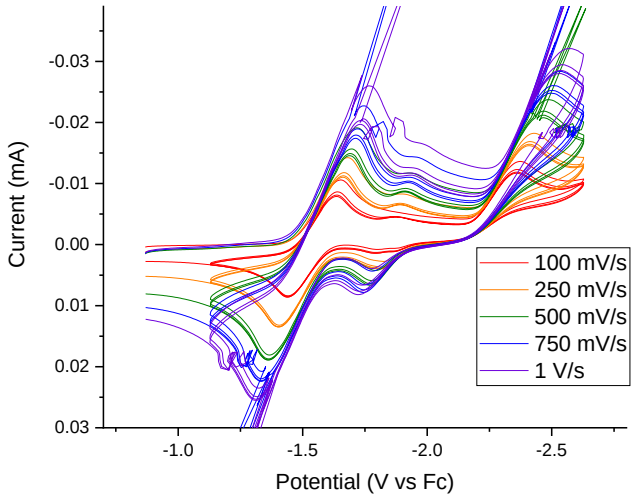

Figure S19. Scan-rate dependence CV of [100FeNO][BPh_4].

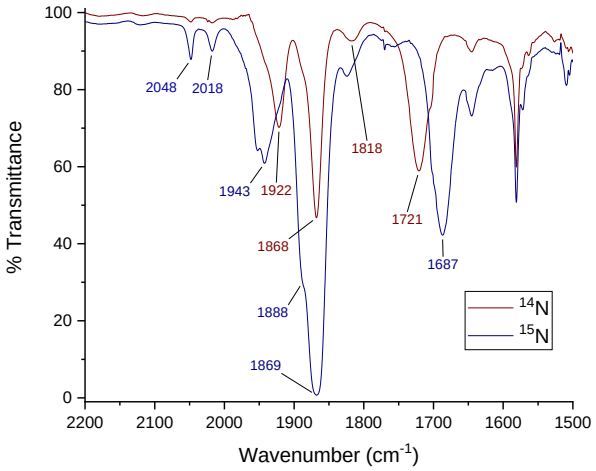

Figure S20. Liquid FT-IRs of labeled and unlabeled NO_3^- reduction reaction mixtures.

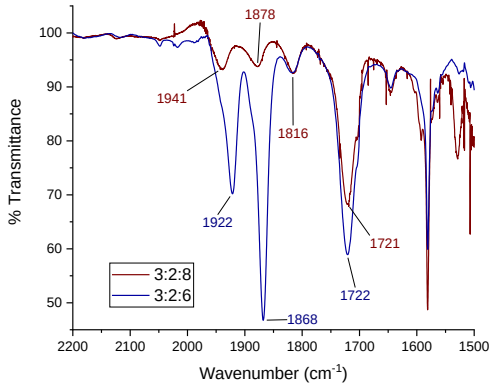

Figure S21. Liquid FT-IRs of PDI:NO_3^-:$[HNEt_3][BPh_4]$ Reactions.

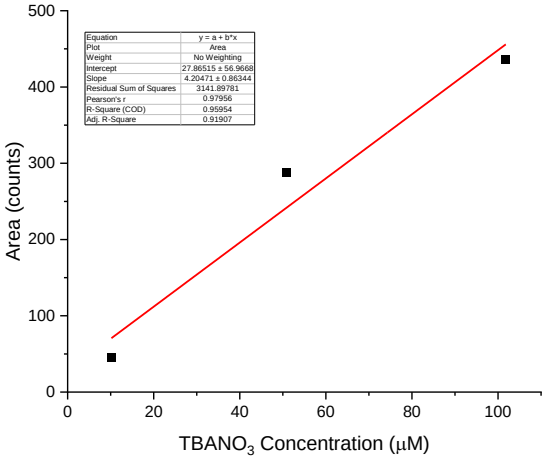

Figure S22. UV-Vis spectra of $[100FeNO][BPh_4]$ standards in THF.

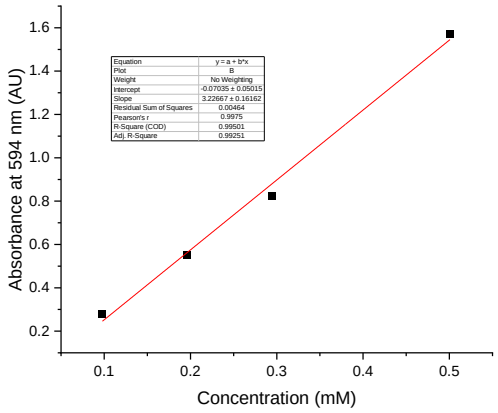

Figure S23. UV-Vis [100FeNO][BPh_4] calibration curve. Linear fit parameters, slope: 3.2, intercept: -0.07, R^2: 0.995.

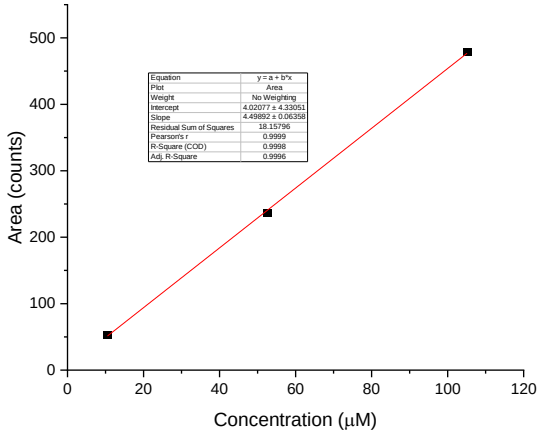

Figure S24. HPIC $TBANO_3$ calibration curve. Linear fit parameters, slope: 4.5, intercept: 4.02, R^2: 0.9998.

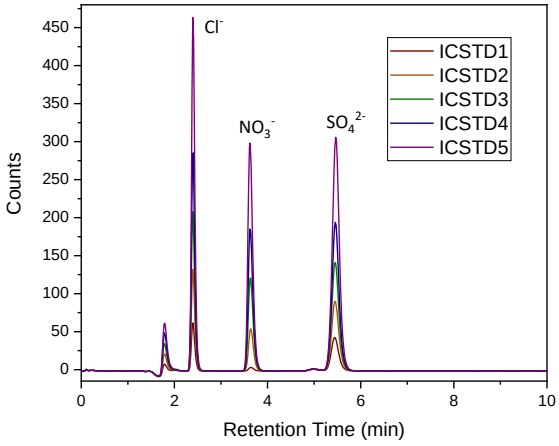

Figure S25. Ion chromatography standard of F^-, Cl^-, NO_3^-, and SO_4^- in nanopure water.

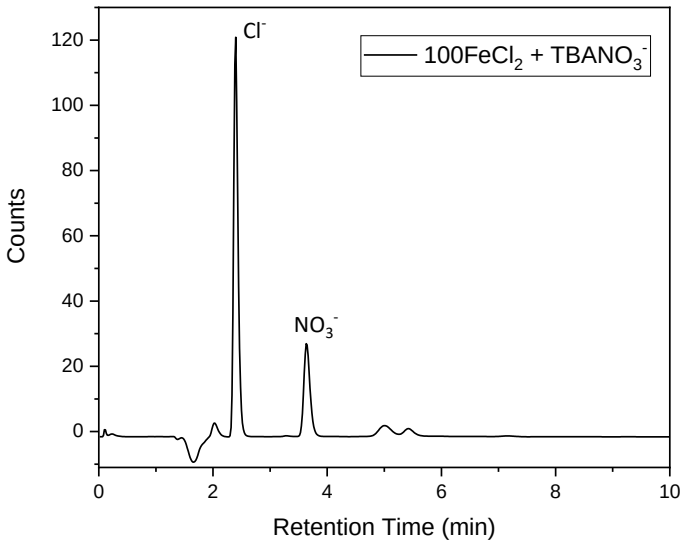

Figure S26. HPIC of $100FeCl_2 + TBANO_3$.

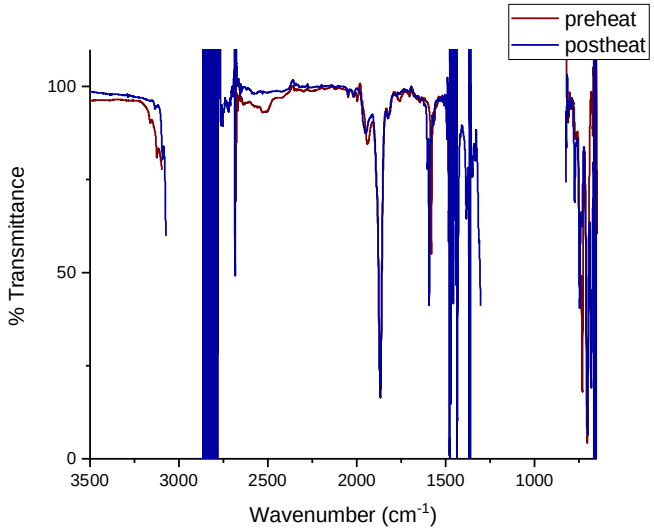

Figure S27. IR of 100FeCO and acid mixture before and after heating.